PRACE INSTYTUTU ODLEWNICTWA
Tom LI Rok 2011 Zeszyt 1
DOI: 10.7356/iod.2011.4

MICROSTRUCTURE EVOLUTION DURING PERITECTIC L + $Al_6Mn(Fe)$ → α-Al + α-AlMnFeSi PROCESS IN AlFeMnSi ALLOYS

EWOLUCJA MIKROSTRUKTURALNA PODCZAS PRZEMIANY PERYTEKTYCZNEJ: L + $Al_6Mn(Fe)$ → α-Al + α-AlMnFeSi W STOPACH AlFeMnSi

Małgorzata Warmuzek

Zespół Laboratoriów Badawczych, Instytut Odlewnictwa, Kraków

Abstract

In this work, the course of peritectic L + $Al_6Mn(Fe)$ → α-Al + α-AlMnFeSi transformation taking place in AlFeMnSi alloys was traced. The specific microstructural effects in the transformed primary phase areas were revealed and identified. The transformation product situated inside the primary preperitectic Al_6FeMn phase precipitates was identified as a lamellar mixture of the α-AlFeMnSi and α-Al phases, balanced volumetrically. The evolution of morphology in a peritectic α-AlMnFeSi phase observed in the examined specimens was related to the necessary exchange of components at interfaces, which are the site for nucleation and growth of transformation products. Both direction and range of the diffusion fluxes of individual components were identified. The distribution of transition metals between intermetallic phases during the progressing transformation was estimated and found to be related to both partition coefficient of components and alloy composition.

Keywords: aluminium alloy, intermetallic phase, transition metals, peritectic transformation, microstructure

Streszczenie

W pracy przedstawiono przebieg przemiany perytektycznej L + $Al_6Mn(Fe)$ → α-Al + α-AlMnFeSi. Przedstawiono zidentyfikowane, towarzyszące jej specyficzne efekty mikrostrukturalne w mikroobszarach przekształconej fazy pierwotnej. Produkt przemiany usytuowany w obrębie pierwotnego wydzielenia fazy Al_6FeMn stanowi mieszaninę faz α-AlFeMnSi i α-Al zbilansowaną objętościowo. Ewolucja morfologiczna fazy α-AlFeMnSi obserwowana w badanych próbkach została odniesiona do procesu wymiany składników między fazami na powierzchniach międzyfazowych, które są miejscem zarodkowania i wzrostu produktów przemiany. Zidentyfikowano kierunek i zakres strumienia dyfuzyjnego pierwiastków wchodzących w skład faz uczestniczących w przemianie. Oszacowano dystrybucję metali przejściowych pomiędzy fazy międzymetaliczne powstające w kolejnych stadiach krystalizacji w zależności od współczynnika podziału i składu stopu.

Słowa kluczowe: stopy aluminium, fazy międzymetaliczne, metale przejściowe, przemiana perytektyczna, mikrostruktura

1. Introduction

The invariant peritectic transformation:

$$L + Al_6Mn \rightarrow \alpha\text{-AlMnSi} + \alpha\text{-Al}$$

Occurring in an Al-Mn-Si system (Fig. 1a) [1] has been identified as a monovariant one in the quaternary Al-Fe-Mn-Si alloys with 1–3% Si content (Fig. 1b) [2-6].

Both of the involved intermetallic Al_6MnFe and α-AlMnFeSi phases are considered to be the solid solutions of Fe in the basic crystals of Al_6Mn and α-AlMnSi structures, respectively.

According to the Al-Fe-Mn-Si equilibrium diagram, when the Si content in AlFe1Mn1Si alloys exceeds 2 wt.%, the transformation of an Al_6MnFe phase ought to be completed and the α-AlMn(Fe)Si phase will be the only stable constituent below 630°C (Fig. 1b).

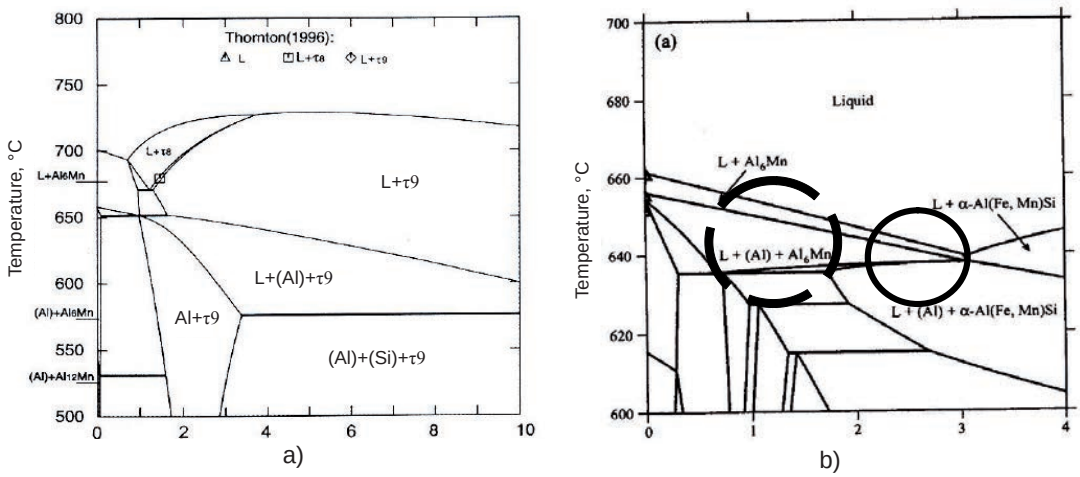

Fig. 1. Equilibrium diagrams with concentration field of peritectic L + $Al_6Mn(Fe) \rightarrow \alpha$-AlMn(Fe)Si transformation; a) polythermal section of Al-4%Mn-Si [1], b) polythermal section of Al-1%Mn1%Fe-Si [4]

Rys.1. Wykresy równowagi faz z zaznaczonymi obszarami stężenia pierwiastków podczas przemiany perytektycznej L+$Al_6Mn(Fe) \rightarrow \alpha$-AlMn(Fe)Si; a) politermiczny przekrój fazy Al-4%Mn-Si [1], b) politermiczny przekrój fazy Al-1%Mn1%Fe-Si [4]

The process of Al_6MnFe phase transformation into the α-AlMnFeSi phase precipitates in technical alloys from the 3xxx series during homogenisation was analysed in detail in the works of Alexander et al. [7–10]. On the ground of the specific microstructural features, some similarity in process mechanism to the lamellar eutectoid formation has been found.

The microstructure evolution effects of an interaction between the two intermetallic phases of Al_6MnFe and α-AlMnFeSi with participation of the α-Al liquid solution were not recognised in full detail, although they have been noticed to run along the crystallisation path of technical aluminium alloys.

Especially, the morphology characteristics of the peritectic $L + Al_6MnFe \rightarrow \alpha$-AlMnFeSi + α-Al transformation products have not been as yet examined in detail, all being non-identifiable by means of the volumetric analytical methods, e.g. calorimetry or X-ray

diffractometry. The specific interface morphology and microstructural features inside the peritectic transformation products can be revealed only by *in situ* methods, such as microscopic observations assisted by either EDS or EBSD analysis. In this work, the microstructural effects of the intermetallic Al_6MnFe and α-AlMnFeSi phases interaction taking place on the solidification path of AlMnFeSi alloys have been described and analysed.

2. Experimental

The examined materials were synthetic AlMnFeSi alloys of composition presented in Table 1. They were melted from pure components in an induction furnace under the protective Ar atmosphere, and were poured next into graphite crucibles.

Table 1. Chemical composition of the examined alloys (Al balance), wt. %

Tabela 1. Skład chemiczny badanych stopów (Al jako reszta), % wag.

Alloy	Si	Mn	Fe	Fe/Mn
AlSi0.5Mn2Fe1.5	0.5	2.0	1.5	0.75
AlSi0.5Mn2Fe2.5	0.5	2.0	2.6	1.30
AlSi2.5Mn2Fe1.5	2.5	2.0	1.5	0.75
AlSi2.5Mn2Fe2.5	2.5	1.8	2.6	1.41

The microstructure evolution and the solidification path as related to alloy composition were analysed in the following specimens:

- after continuous cooling in as-cast state (poured to graphite crucible),
- cooled slowly, i.e. at a rate of 5 K/min, from liquid state to 500°C (the programmed mode in DSC calorimeter).

The specimens of alloys 1 and 3 were also held at a temperature of 630°C for 2 and 4 h to reveal the range of progress in transformation.

Microstructure observations were carried out using both Axio Observer Z1m metallographic light microscope and STEREOSCAN 420 scanning electron microscope.

The thermal effects of the processes occurring during solidification were recorded with a DS Netzsch 402E calorimeter. Local chemical composition of the microstructural constituents and elements distribution were estimated by means of the EDS microanalysis with LINK ISIS system. The intermetallic phases were identified *in situ* by means of the EBSD method.

In the carried out experiments, the microstructure evolution analysis was limited to chosen microregions of the peritectic transformation layers, situated in individual complex precipitates (Fig. 2).

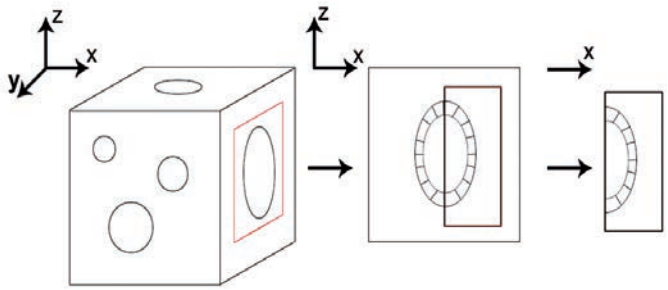

Fig. 2. Microstructure area under consideration as situated in a specimen of the volumetrically solidifying alloy

Rys. 2. Badany obszar mikrostruktury zlokalizowany w próbce stopu krzepnącego objętościowo

3. Results and discussion

3.1 Microstructural effects in the transformed primary phase during continuous cooling

In the examined specimens, solidification starts with precipitation of the primary $Al_6Mn(Fe)$ phase followed by a peritectic process. The transformed areas are situated within the previous profile of the primary phase. Therefore, final shape of the transformed constituents reflects that of the primary precipitates formed at the beginning of the process (Fig. 3). Progress in the transformation was influenced by Si content. In both as-cast hypo-peritectic (0.5% Si) and near-peritectic (2.5% Si) alloys, the primary $Al_6Mn(Fe)$ phase precipitates coated with transformation products prevailed in the microstructure, although an important non-equilibrium fraction of the thermodynamically unstable Al_6MnFe phase also remained there (Figs. 1a and 3a, 1b and 3 b). In the near-peritectic alloy, the separated α-AlMnFeSi phase polyhedra directly precipitated from the liquid were also present (Fig. 3b). The eutectic $L \rightarrow \alpha\text{-Al} + \alpha\text{-AlMnFeSi} + (Si)$ transformation was the final process on a solidification path [1].

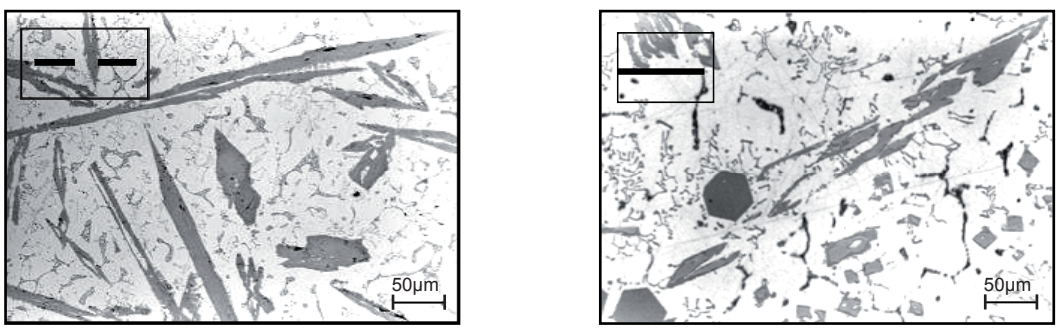

a) b)

Fig. 3. Microstructure of AlMnFeSi alloys poured into graphite crucible, LM, 200x, etched with 1% HF; a) alloy 1-hypoperitectic, b) alloy 3-near peritectic (fields of respective Si concentration in alloy marked by adequate lines in Fig. 1b)

Rys. 3. Mikrostruktura stopów AlMnFeSi odlewanych do tygla grafitowego, mikroskopia świetlna, pow. 200x, trawienie 1%HF; a) stop 1-podperytektyczny, b) stop 3-okołoperytektyczny (zakresy stężenia Si w stopie oznaczone odpowiednimi liniami na rys. 1b)

However, in contrast to the layer usually observed during peritectic solidification, the layer of peritectic products in the examined specimens was composed of the branched plates, arranged in segments similar to those present in either eutectoid or eutectic structure (Fig. 4). The lamellar morphology revealed in the specimens after deep etching (Fig. 4b) was almost identical to that formed after annealing treatment in the solid state, observed by Alexander [7–10] in the 3xxx series alloys and by Li and Arnberg [11] in the 5xxx series alloys.

The results of the X-ray microanalysis have shown an important difference in the Si content between monophase centre and two-phase periphery (Fig. 4a) of the complex massive particles. The EBSD analysis allowed identification of phase components present in these microregions: the Al_6FeMn phase – in the centre, and a mixture of the α-AlMn(Fe)Si phase and α-Al solid solution – in the periphery.

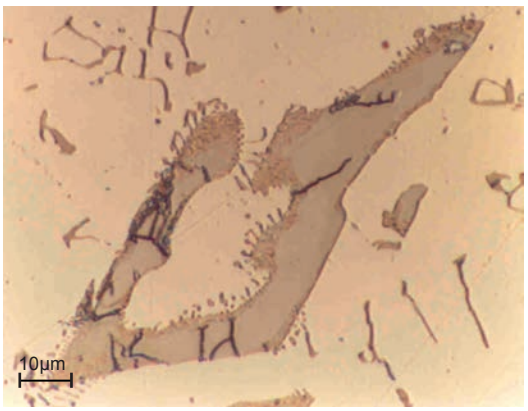

a)

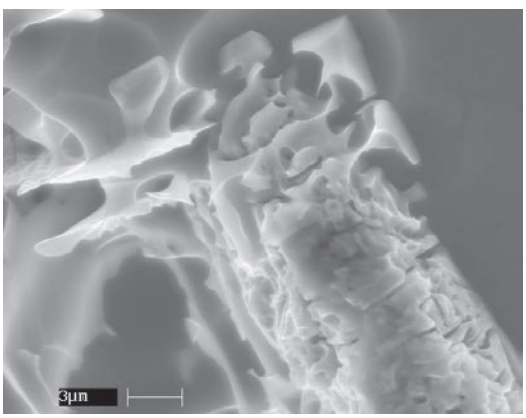

b)

Fig. 4. Morphology of the transformed Al_6FeMn particle in alloy 1, as-cast state; a) separated fields of the peritectic transformation products in a partially transformed Al_6FeMn particle, LM, etched with 1% HF, 800x, Al_6FeMn primary precipitates with transformation products, b) morphology on the external surface of transformation products, SEM, etched with NaOH, 3500x

Rys. 4. Morfologia cząsteczki Al_6FeMn po przemianie w stopie 1, stan surowy po odlaniu; a) poszczególne obszary produktów niepełnej przemiany perytektycznej w cząsteczce Al_6FeMn, mikroskopia świetlna, trawienie 1% HF, pow. 800x, wydzielenia pierwotne Al_6FeMn z produktami przemiany, b) morfologia zewnętrznej powierzchni produktów przemiany, SEM, trawienie NaOH, pow. 3500x

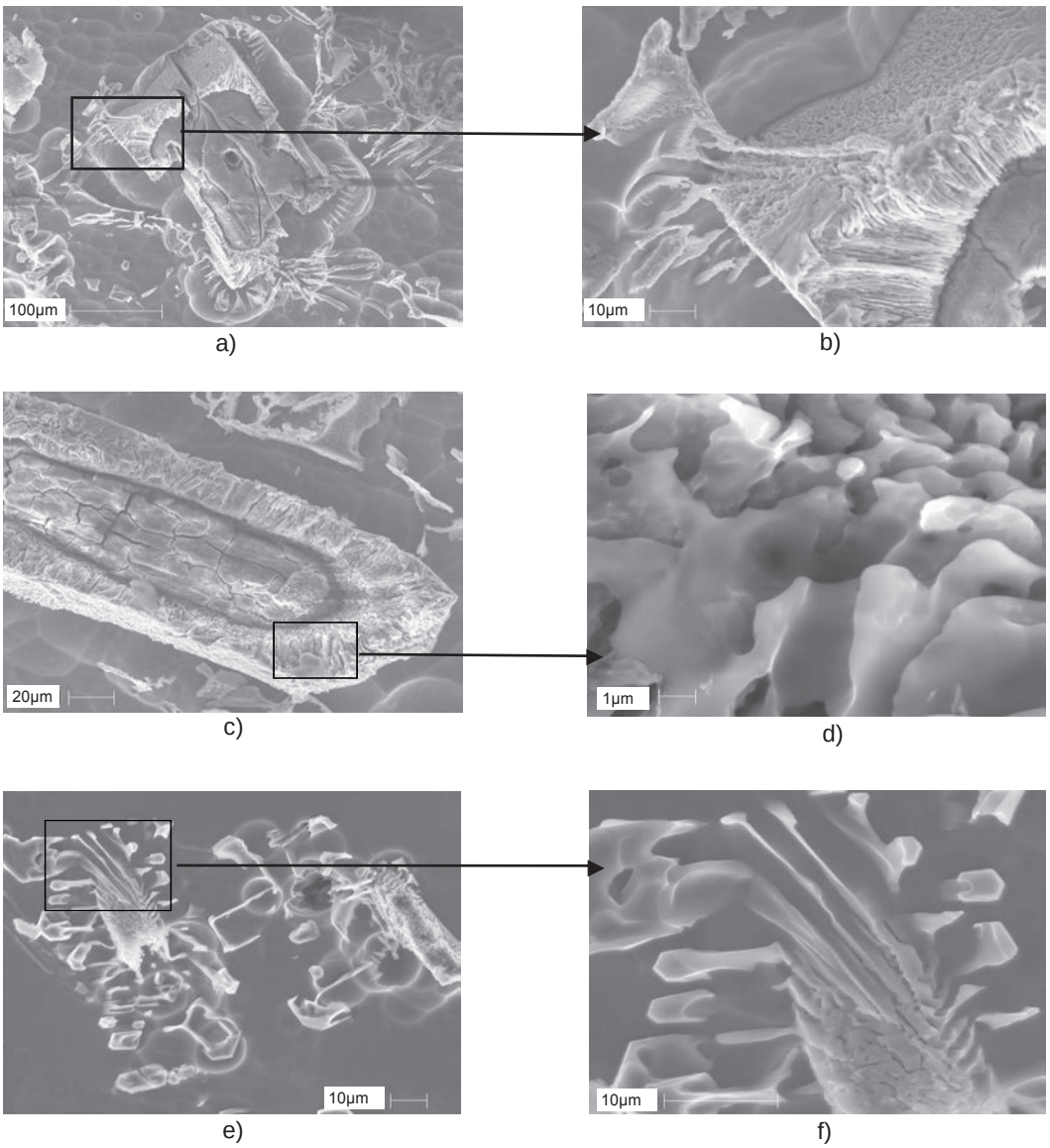

Fig. 5. Morphology of the α-AlFeMnSi phase as affected by alloy composition, specimens frozen after annealing at 630°C/2 h, SEM, deep etched with NaOH, a) alloy 1, 200x, b) enlarged microregion from Fig. 8a, 1200x, c) alloy 2, 800x, d) enlarged microregion from Fig. 8c, 9000x, e) alloy 4, 800x, f) enlarged microregion from Fig. 8e, 3000x

Rys.5. Morfologia fazy α-AlFeMnSi w zależności od składu stopu, próbki chłodzone po wyżarzaniu w temperaturze 630°C/2 h, skaningowa mikroskopia elektronowa, głębokie trawienie NaOH, a) stop 1, pow. 200x, b) powiększony mikroobszar pokazany na rysunku 8a, pow. 1200x, c) stop 2, pow. 800x, d) powiększony mikroobszar pokazany na rysunku 8c, pow. 9000x, e) stop 4, pow. 800x, f) powiększony mikroobszar pokazany na rysunku 8e, pow. 3000x

Though the dispersion of two-phase mixture does not allow us to unequivocally decide about the presence of an α-Al solid solution, some indirect proofs can support this assumption:

- the Al-Mn-Fe-Si equilibrium diagram [2–5],
- the particle morphology after deep etching in a reagent solving the Al matrix (Figs. 4, 5),
- the results of EELS analysis of particles produced during transformation accompanying the heat treatment of 3xxx series alloys [7],
- the chemical balance of components in a unit volume of the transformed material: $3Al_6MnFe + 2Si = Al_{15}(MnFe)_3Si_2 + 3Al$ [7].

In an Al-Mn-Fe-Si system, besides the monovariant transformation mentioned in the introduction, two invariant peritectic reactions can occur:

$L + Al_6MnFe + Al_3Fe \rightarrow$ α-Al + α-AlMnFeSi [2]

$L + Al_6MnFe \rightarrow$ α-Al + $Al_{13}Fe_4$ + α-AlMnSi [5].

Since the presence of the $Al_{13}Fe_4$ phase has not been detected in composed, polyphase particles observed in the examined specimens, a polyphase microstructure like that visible in Figs. 3–6 was considered to be a product of monovariant peritectic transformation, expected according to Al-Mn-Fe-Si equilibrium diagram presented by Phragmen [2]:

$L + Al_6MnFe \rightarrow$ α-Al + α-AlMnFeSi.

The peritectic zones formed in 0.5% Si alloys at the external α-AlMnFeSi/α-Al interface were enclosed with a homogenous layer of the α-AlMnFeSi phase of different thickness (Fig. 6a), while the external filigrees, though sometimes observed, were very short and slightly branched. This mechanism of microstructure evolution in the external layer can be attributed to either coalescence or Ostwald ripening [7, 8]. These are the thermodynamically-driven processes occurring because particles of larger size are more energetically favoured than the smaller ones. The morphology of a transition zone between the layers (lamellar two-phase and monolithic) indicates that larger particles continue to grow at the expense of smaller ones, which would rather suggest Ostwald mode of ripening (Figs. 6, 10).

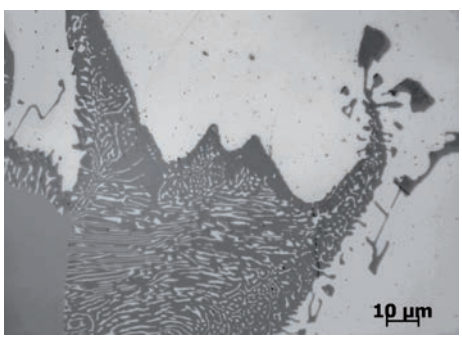

a)

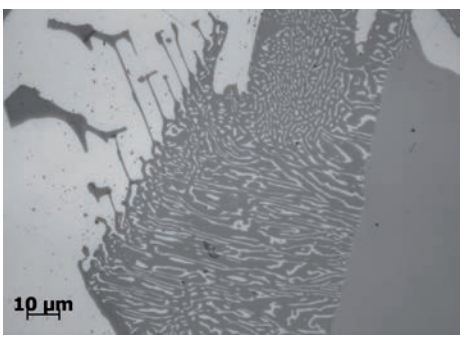

b)

Fig. 6. Morphology of the α-AlMn(Fe)Si phase precipitates formed during peritectic transformation; LM, etched with 1% HF, 1000x, cooling rate of 5 K/min; a) alloy 2, b) alloy 4

Rys. 6. Morfologia wydzieleń fazy α-Mn(Fe)Si powstałych podczas przemiany perytektycznej; mikroskopia świetlna, trawienie 1% HF, pow. 1000x, szybkość stygnięcia 5 K/min; a) stop 2, b) stop 4

The lamellar morphology of two-phase layer is of a rather regular character, especially in frozen specimens (Figs. 5 a–d), although some fluctuations in either spacing or orientation are also visible (Figs. 5 e–f, 6). The measured length of peritectic lamellae has reached value comparable with thickness inside of the the peritectic layer (Figs. 5a–d, 6b).

Instead, the zone of the Chinese script filigrees outside the primary particles profile has very distinct features of the peritectic complex particles produced in 2.5% Si alloys. More detailed observations have revealed a close interrelation between the external α-AlMnFeSi phase precipitates and some lamellae in a two-phase layer. Their branched shape can suggest that they started growing in liquid alloy still before the α-Al matrix has started to solidify (Fig. 5b, 6e–f).

3.2. Model of microstructure evolution during the $Al_6MnFe \rightarrow$ α-AlMnFeSi phase transformation in liquid Al-alloy

3.2.1. Peritectic crystallisation mechanism

The process of peritectic microstructure formation consists of the three main stages [12–14]:

1. nucleation of peritectic phase at the $L/Al_6MnFe/\alpha$ interface,
2. peritectic reaction – when the triple-point junction of $L/Al_6MnFe/\alpha$-AlMnFeSi exists,
3. peritectic transformation – when the L/Al_6MnFe interface becomes covered with reaction products.

The specific microstructure observed in peritectic alloys is strongly affected by interactions at the interfaces subordinated to the peritectic mechanism rules.

At the initial stage, at a temperature T_p, the three phases of Al_6MnFe, α-AlMnFeSi and L have to co-exist in the state of equilibrium. With a decrease of temperature, at $T < T_p$, when the system tends to lower its overall energy, the Al_6MnFe phase starts dissolving, while the new α-AlMnFeSi phase starts to grow. The driving force for that process results from the Gibbs potentials difference: $\Delta G = G_{Al6MnFe} - G_{\alpha-AlMnFeSi}$ (Fig. 7).

a) peritectic model: $Al_6 + L \rightarrow \alpha_c + Al$

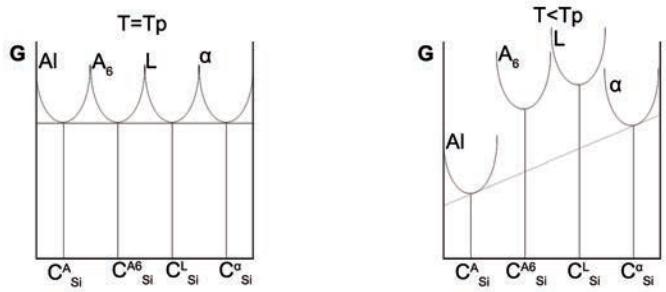

b) eutectoid model: $Al_6 \rightarrow \alpha_c + Al$

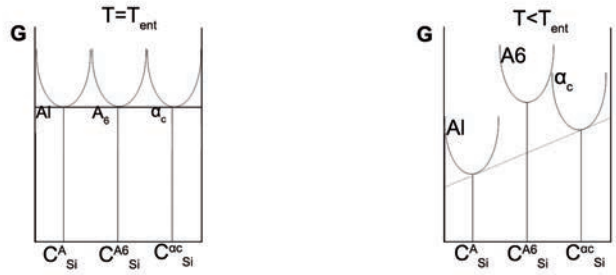

Fig. 7. Free energy in Al_6MnFe-α-AlMnFeSi-α-Al system during the L + $Al_6MnFe \rightarrow$ α-AlMnFeSi + α-Al transformation; a) peritectic model, b) eutectoid model; (common G vs CSi relationships simplified for considered transformation)

Rys. 7. Energia swobodna w układzie Al_6MnFe-α-AlMnFeSi-α-Al podczas przemiany L+$Al_6MnFe \rightarrow$ α-AlMnFeSi + α-Al; a) model perytektyczny, b) model eutektoidalny (zwykłe współzależności pomiędzy G i CSi uproszczone dla omawianej przemiany)

The Alexander theory of two-phase product formation induces a comparison between some particular characteristics of both peritectic and eutectoid transformations [7, 8]. Though phase evolution in alloy caused by both processes, i.e. eutectoid and $Al_6FeMn \rightarrow$ α-AlMnFeSi, does have some points in common (Fig. 7), a comparison of the content of components in a unit volume before and after both transformations makes the essential difference between them well visible (Fig. 8). During eutectoid transformation (e.g. perlitic), the average composition in a unit volume is stable and the necessary transfer of components is limited to an interlamellar distance only (Fig. 8a), while during the $Al_6FeMn \rightarrow$ α-AlMnFeSi process, the strong Si deficiency at the transformation front has to be made up to achieve a concentration level adequate for the α-AlFeMnSi phase to exist (Fig. 8b). Therefore, a modified approach is needed to identify the course of the L + $Al_6MnFe \rightarrow$ α-AlMnFeSi + α-Al transformation during alloy solidification.

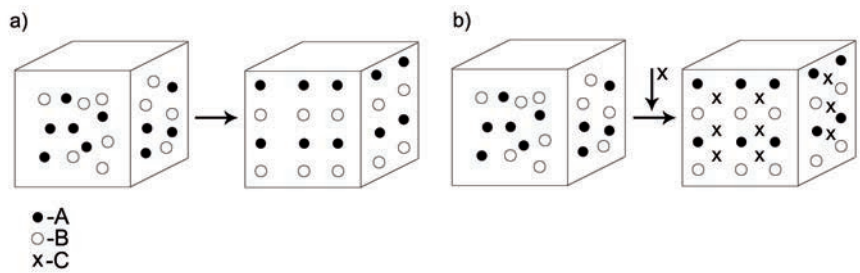

Fig. 8. Mass balance in a unit volume of the two-phase α-AlMnFeSi+α-Al cell; components` atoms distribution specific to particular transformation models; a) eutectoid AB → B + A transformation, b) Al_6MnFe + L → α-AlMnFeSi + α-Al (A-Al, B-TM; Fe+Mn, C-Si)

Rys. 8. Bilans masy w jednostkowej objętości komórki dwufazowej α-AlMnFeSi+α-Al; rozkład atomów składników charakterystyczny dla danego modelu przemiany; a) przemiania eutektoidalna AB → B + A, b) przemiana Al_6MnFe + L → α-AlMnFeSi + α-Al (A-Al, B-TM; Fe+Mn, C-Si)

3.2.2. The α-AlMnFeSi phase nucleation

The results of the present work and of the studies carried out previously [9, 15–17] have allowed to recognise the $Al_6FeMn/(L)$ interface as a favourable substrate for the peritectic phase nucleation.

Watanabe`s results [18] obtained for technical alloys have shown that the activation energy of α-AlMnFeSi phase nucleation during the solid state $Al_6MnFe \rightarrow$ α-AlMnFeSi transformation is strongly influenced by Si concentration (Table 2).

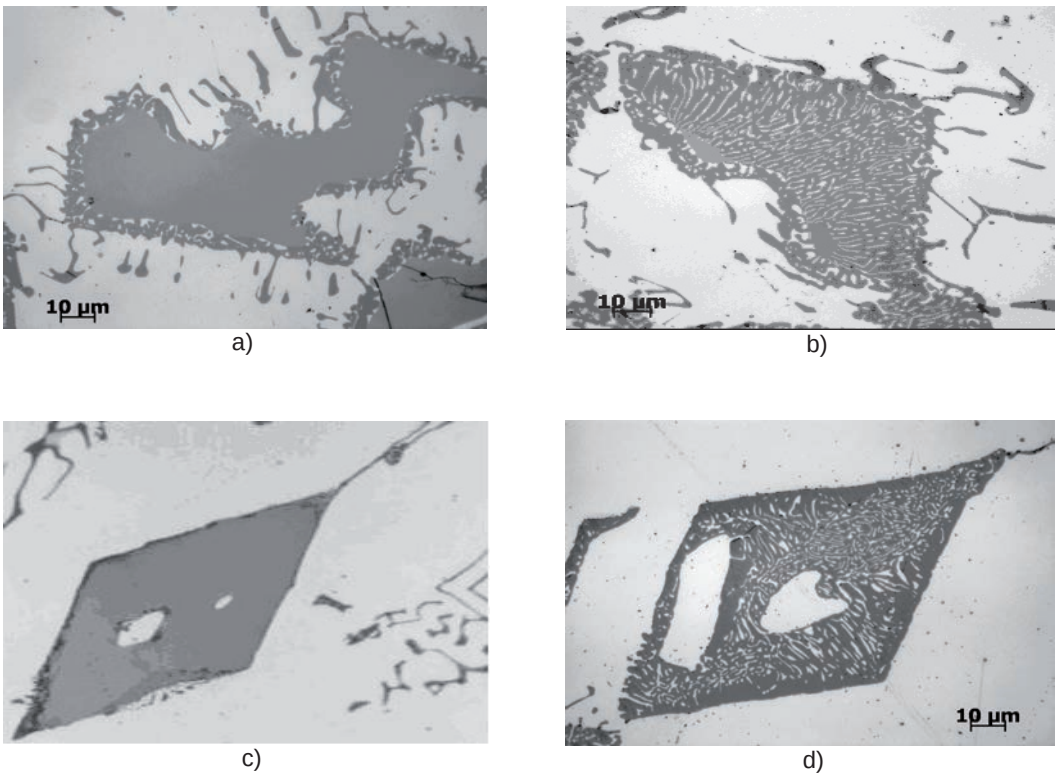

Fig. 9. The distribution of α-Al(MnFe)Si phase nuclei at the $Al_6FeMn/(L)$ interface, LM, 1000x, etched with 1% HF; a) alloy 4, after annealing at 630°C/1 h, cooled to ambient temperature, the nuclei of α-Al(MnFe)Si phase uniformly distributed at the $Al_6FeMn/(L)$ interface, b) alloy 4 after annealing at 630°C/4 h, the transformed particle with two-phase area formed at one of the primary precipitate facets, c) alloy 1, cooled 5 K/min, to ambient temperature, the peritectic process has originated in two separated microregions at the $Al_6FeMn/(L)$ interface, d) alloy 1 after annealing at 630°C/1 h, the transformed particle with two-phase areas originating from 4 nuclei

Rys. 9. Rozkład zarodków fazy α-Al(MnFe)Si na powierzchni rozdziału faz $Al_6FeMn/(L)$, mikroskopia świetlna, pow. 1000x, trawienie 1% HF; a) stop 4 po wyżarzaniu w temperaturze 630°C/1 h, chłodzenie do temperatury otoczenia, zarodki fazy α-Al(MnFe)Si równomiernie rozłożone na powierzchni rozdziału faz $Al_6FeMn/(L)$, b) stop 4 po wyżarzaniu w temperaturze 630°C/4 h, cząsteczka po przemianie z głównym obszarem dwufazowym utworzonym na jednej z płaszczyzn wydzielenia, c) stop 1 po wyżarzaniu w temperaturze 630°C/1 h, d) cząsteczka po przemianie z obszarami dwufazowymi utworzonymi z 4 zarodków

Table 2. The activation energy for α-AlMnFeSi phase nucleation in 3xxx series alloys (acc. to Arrhenius formula: (t) = f(1/T) [18,19]

Tabela 2. Energia aktywacji potrzebna dla zarodkowania fazy α-AlMnFeSi w stopach z serii 3xxx (wg wzoru Arrheniusa: (t)=f(1/T) [18,19]

Alloy	Si0.35Fe0.50Mn1.08	Si0.21Fe0.55Mn1.07	Si0.18Fe0.5Mn1.06
Activation energy, kcal/mole	60+/-10	67	90

Similar relationships can be assumed to exist in the process with liquid alloy participation, all the more that in the examined specimens of 2.5% Si alloys undercooled to 630°C, the α-AlMnFeSi phase nuclei have been distributed uniformly (Fig. 9a), while in the specimens of 0.5% Si alloy only several isolated peritectic zones have been formed on the surface of the primary precipitates (Figs. 4a, 9c).

The transformed areas developed from these isolated nuclei differed in both spatial and crystallographic orientation of the α-AlMnFeSi particles (Figs. 9d, 10). This fact can testify that close crystallographic relationships between the primary and peritectic intermetallic precipitates have not been formed. Within the whole transformed area, the α-AlMnFeSi lamellae regular and of parallel orientation (shown in Fig. 9b) were observed to occur only incidentally.

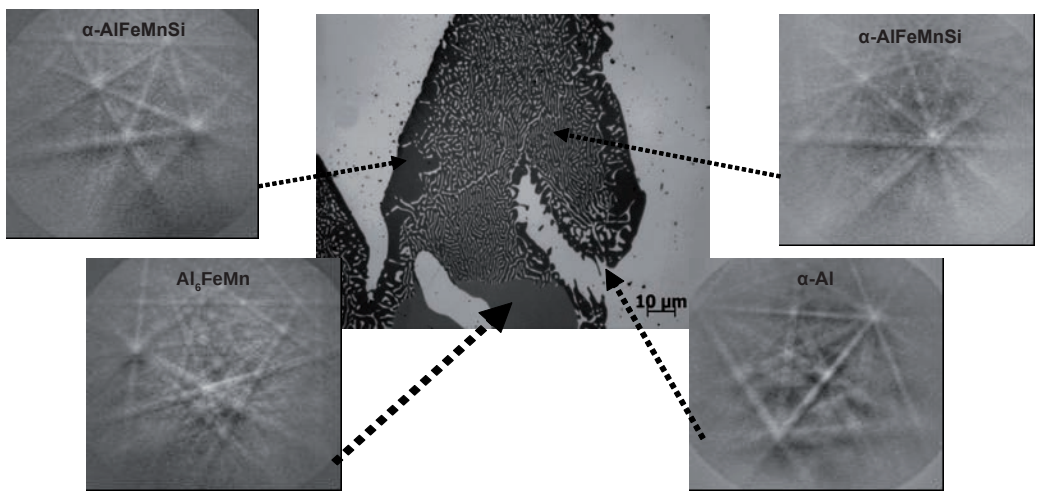

Fig. 10. Peritectic transformed zone composed of microregions with different orientations of the α-AlMnFeSi phase precipitates, alloy 1, LM, etched with 1% HF, 1000x (EBSD patterns situated at points marked in the micrograph)

Rys. 10. Strefa przemiany perytektycznej składająca się z mikroobszarów o różnym ułożeniu wydzieleń fazy α-AlMnFeSi, stop 1, mikroskopia świetlna, trawienie 1% HF, pow. 1000x (obrazy EBSD zlokalizowane w punktach zaznaczonych na mikrografii)

The critical radius of the heterogeneous nucleus is smaller than that of a homogeneous one, and therefore it can start growing at lower undercooling. The non-uniform distribution of nuclei observed in the examined alloys can signify constantly high energy barriers in spite of the actual thermodynamic preference.

According to the nucleation theory, the critical radius of nucleus r_{crit} [20, 21] capable to grow:

$$r_{crit} = \frac{2T_p \gamma}{\Delta T \, \Delta H}$$

(where: ΔH − transformation enthalpy, ΔT − undercooling) is influenced by the superficial energy γ.

Thus, relatively high energy activating the nucleation of peritectic phase results from the high value of the surface factor γ. As both intermetallic phases have different crystal symmetry and elementary cell size, the significant crystal lattice misfit at the substrate/ nucleus interface can increase the energetic barrier for the formation of a nucleus capable to grow.

Another distinctive feature of the nucleation course has also been observed. Quite often, the peritectic transformed areas are situated on the corners of the primary Al_6MnFe precipitates (Figs. 4a, 9c–d) while, according to the heterogeneous nucleation theory, the critical radius of nuclei formed on a convex surface tends to be larger than in the case of a plane [20, 22]. However, this spatial nucleation preference represents some analogy to that observed in homogenised solid alloys.

On the other hand, the completely untransformed primary Al_6FeMn precipitates, observed previously in alloy 3004 after long-lasting heat treatment, have not been detected now, even in hypo-peritectic alloys [9–10].

3.2.3. The formation of peritectic layer

Simultaneously to the α-AlMnFeSi phase nuclei arising at the $Al_6Mn(Fe)$/α-Al interface, a closely attached microregion of the α-Al solid solution is formed. Though nucleation priority has not been settled yet, further growth of the peritectic layer is not possible before a two-phase cell is formed. The relationships between the crystallographic orientations of α-AlFMnSi and α-Al lamellae within a two-phase layer have not been established until now, as stated for the α-AlFMnSi dispersoids precipitated directly in the Al matrix [23]. Alexander has revealed the presence of a common continuous orientation of the α-Al solid solution occurring after solid state transformation in both the transformed lamellae and surrounding matrix [7, 8].

The range of transformation in specimens frozen in the state below the equilibrium temperature has been rather limited. Only due to prolonged holding below the transformation temperature, an advanced progress as visible in the specimens presented in Figs. 9b and d has been achieved.

According to the classic theory of peritectic solidification in binary systems [12–14], at a temperature T_p both solid phases co-exist in direct contact and the necessary exchange of constituents takes place within the liquid phase.

In Figure 11, particular stages of microstructure evolution typical for peritectic solidification can be identified:

- point n – nucleation of α-AlFeMnSi phase at the L/Al_6MnFe interface, the start of peritectic reaction (Fig. 11a),
- line l – peritectic reaction in progress along the L/Al_6MnFe interface (Figs. 11a and b),
- line p – peritectic transformation in progress perpendicular to the L/Al_6MnFe interface (Figs. 11a and b),
- point e – the end of peritectic reaction (Fig. 11b).

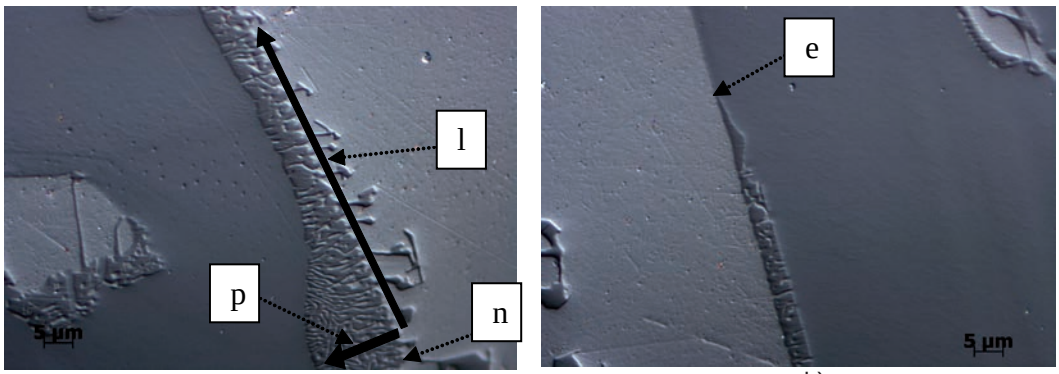

a) b)

Fig. 11. Peritectic layer in the peritectic alloy 4, LM, DIC, etched with 1% HF, 1600x; a) microregion of the α-AlFeMnSi phase nuclei formation, b) microregion of the process end, a triple-point junction visible (point n – the start of the nucleation of α-AlFeMnSi phase at the L/Al_6MnFe interface, line l – peritectic reaction in progress along the L/Al6MnFe interface, p – line of the transformation progress perpendicular to L/Al_6MnFe interface, point e – the end of peritectic reaction)

Rys. 11. Warstwa perytektyczna w perytektycznym stopie 4, mikroskopia świetlna, kontrast Nomarskiego, trawienie 1% HF, pow. 1600x; a) mikroobszar tworzenia zarodków fazy α-AlFeMnSi, b) mikroobszar końca procesu; widoczny punkt potrójny (punkt n – początek zarodkowania fazy α-AlFeMnSi na powierzchni rozdziału faz L/Al_6MnFe, linia l – przemiana perytektyczna postępująca wzdłuż powierzchni rozdziału faz L/Al_6MnFe, p – linia znacząca przebieg przemiany prostopadła do powierzchni rozdziału faz L/Al_6MnFe, punkt e – koniec przemiany perytektycznej)

To describe the formation of a peritectic layer visible in Fig. 11, a lateral model of the peritectic growth [14] has been adopted (Fig. 12).

From the moment the first nucleus of the new phase is capable to grow ($r > r_{crit}$), further development of the peritectic zone will be the resultant of two partial processes, occurring simultaneously at two interfaces:

1. peritectic reaction:

at the L/Al_6MnFe interface: $Al_6MnFe + Si (L) \rightarrow \alpha\text{-AlFeMnSi} + \alpha\text{-Al} + L`$.

The movement of the triple-point L/Al_6MnFe/α-AlFeMnSi junction is parallel to the surface of the primary precipitates, where the α-AlFeMnSi phase nuclei are successively formed, owing to the supply of Si atoms from the liquid alloy, and Fe and Mn atoms from the superficial Al_6MnFe phase layer:

This process is controlled by the α-AlFeMnSi phase nucleation:

2. peritectic transformation:

at the α-AlFeMnSi/Al_6MnFe interface: $Al_6MnFe + Si (S) \rightarrow \alpha\text{-AlFeMnSi} + \alpha\text{-Al}$.

The movement of the two-phase cell front (α-AlFeMnSi + α-Al) is perpendicular to the primary Al_6MnFe particle surface, where atoms of the transition metals from an Al_6MnFe particle are incorporated *in situ* in the tightly adhering new phase layer, while all the necessary Si atoms have to be transported across the solid layer of increasing thickness.

This process is controlled by Si atoms transport in the solid phase layer:

at α-AlFeMnSi/L : $L` \rightarrow \alpha$–AlFeMnSi + L".

Below the equilibrium temperature, the α-AlFeMnSi phase becomes thermodynamically favoured and can precipitate directly from the liquid alloy, without any contact with the L/Al_6MnFe interface.

This process is controlled by the diffusion transport of either transition metals (Fe and Mn) or Si atoms in the liquid phase.

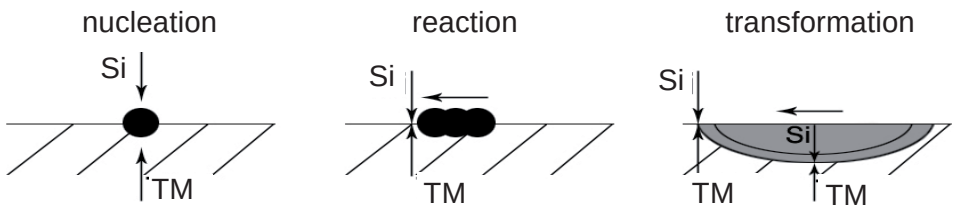

Fig. 12. Microstructural model of peritectic zone formation initiated with triple reaction among the Al_6FeMn, L and α-AlFeMnSi phases (lateral peritectic reaction model [14] adapted to the considered transformation)

Rys. 12. Model mikrostrukturalny powstawania strefy perytektycznej zapoczątkowanej przez potrójną reakcję pomiędzy fazami Al_6FeMn, L i α-AlFeMnSi (model boczny reakcji perytektycznej [14] zaadaptowany do badanej przemiany)

According to Alexander`s analysis, at temperatures used for the 3xxx alloys homogenisation, the transformation is controlled by the nucleation rate of α-Al-MnFeSi phase [8]. However, an increase in the transformed layer thickness due to the specimen undercooling to 630°C below the equilibrium peritectic temperature has been very small in both the examined alloy groups. It means that the Si diffusion transport in solid peritectic layer has limited further progress of transformation at the Al_6FeMn/(α-Al(MnFe)Si interface in a lower temperature range.

3.2.3. The morphology of lamellar microstructure in peritectic zone

The kinetic domination of the newly arising phases has not been observed at the internal front of growth (Figs. 5, 6, 10, 11), which means that some analogy to the lamellar coupled growth can be derived [20]. Thus, the growth of a two-phase cell can be described with the fundamental terms of a discontinuous precipitation theory, assuming that the components transfer takes place only at an interlamellar distance, parallel to the transformation front. In the analysed two-phase layer, these conditions can be satisfied only as regards the transfer of transition metals (Fe and Mn), since they are present in the primary phase in an amount sufficient for the *in situ* building of an α-AlFeMnSi phase plate.

Both peritectic zone thickening and α-AlFeMnSi phase lamellae lengthening can continue provided that the Si transport to the α-AlFeMnSi/Al_6MnFe interface will be sufficient to make up for the concentration deficiency. Therefore, the Si flux perpendicular to the two-phase front plane is necessary for further progress (Figs. 12, 13).

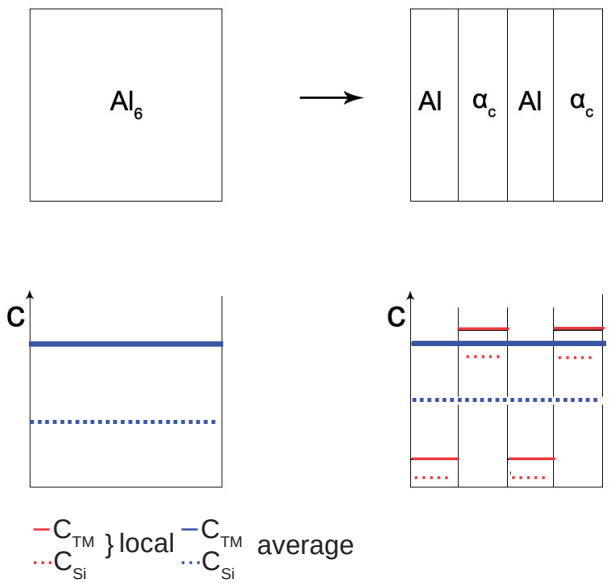

Fig. 13. Components distribution between interacting phases: primary and peritectic, during the $Al_6MnFe \rightarrow \alpha$-AlMnFeSi + α-Al transition (assumptions: in situ process mechanism, mass balance in the transformed microregion $\Delta C = C_{\alpha\text{-AlMnFeSi + a-Al}} - C_{Al6MnFe}$; transition metals (Fe + Mn) balance $\Delta TM = 0$, silicon balance $\Delta Si = 6-8$ wt.%)

Rys. 13. Rozkład składników między interaktywnymi fazami: fazą pierwotną i fazą perytektyczną podczas przemiany $Al_6MnFe \rightarrow \alpha$-AlMnFeSi + α-Al przy następujących założeniach: proces przebiega według mechanizmu in situ, równowaga masy w mikroobszarze po przemianie, $\Delta C = C_{\alpha\text{-AlMnFeSi + }\alpha\text{-Al}} - C_{Al6MnFe}$; metale przejściowe (Fe + Mn) stan równowagi $\Delta TM = 0$, stan równowagi krzemu $\Delta Si = 6-8$ wt.%)

In Zener`s theory of the stationary coupled growth, the interlamellar distance λ is influenced by the rate of the two-phase boundary movement [20, 22, 24].

Brandt`s solution of this problem is expressed by the following formula:

$$V = a\,\frac{D}{\lambda}$$

(where: V – the rate of the two-phase boundary movement, a – complex material constant, D – diffusion constant).

The subsequent transformations lead to the following relationship:

$$\lambda = \frac{4\gamma\, T_p}{\Delta H \Delta T}$$

(where: γ – surface energy, ΔH − transformation enthalpy, ΔT − undercooling).

Therefore, the actual lamellar spacing observed in peritectic zone can be ascribed to local undercooling at the front growth.

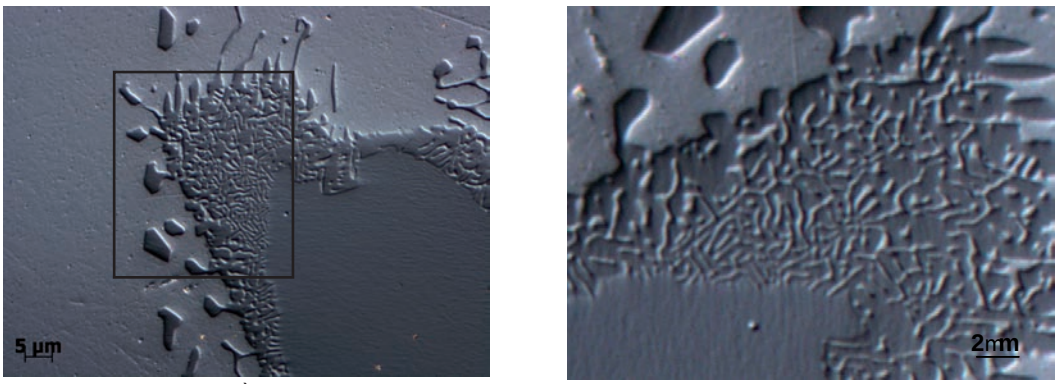

a) b)

Fig. 14. Morphology of the α-AlMnFeSi lamellae, P – in peritectic zone, F – in filigree zone, AlFe1Mn2Si1 alloy, LM-DIC, etched with 1% HF; a) 1000x, b) enlarged microregion from Fig. 10a, 3000x

Rys. 14. Morfologia płytek fazy α-AlMnFeSi, P – obszar perytektyki, F – obszar struktury chińskiego pisma, stop AlFe1Mn2Si1, mikroskopia świetlna, kontrast Nomarskiego, trawienie 1% HF; a) pow. 1000x, b) powiększony mikroobszar z rysunku 10a, pow. 3000x

In the peritectic two-phase layers visible in Figs. 11 and 14, some decrease in lamellar spacing is visible as a distance from the external (α-AlFeMnSi + Al)/α-Al(L) interface has increased. The λ value was two or even three times lower at the internal (α-AlFeMnSi + Al)/Al_6MnFe front, where the growth was arrested, than it was at the external primary precipitate profile. The minimum λ value in all the examined specimens was nearly the same (Table 3).

Table 3. Characteristics of α-AlFeMnSi phase lamellae in the examined alloys

Tabela 3. Charakterystyka płytek fazy α-AlFeMnSi występującej w badanych stopach

Alloys	**0.5 wt. % Si**		**2.5 wt. % Si**	
Spacing, µm	λ_{min}	λ_{max}	λ_{min}	λ_{max}
layer	0.5	1.5	0.5	2.0
filigrees	5	10	3	8

Jackson and Hunt`s principle of the extremum growth [21, 24] allows explaining not only the changes observed in lamellar spacing but also the reason of kinetic limitations for the peritectic zone growth. Progress in the transformation front movement is possible only when λ value belongs to the range of $\lambda_e - \lambda_{max}$, determined by local undercooling and equilibrium diagram characteristics.

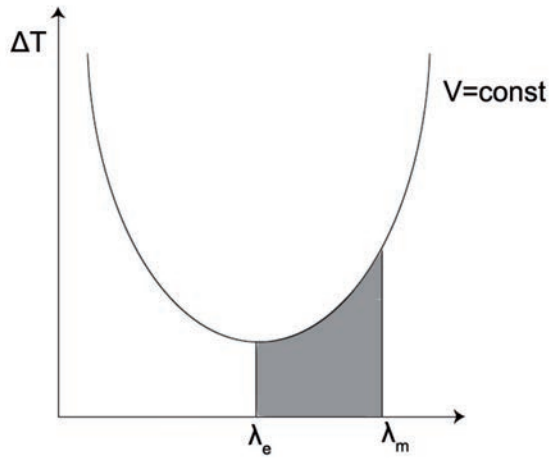

Fig. 15. Undercooling of the two-phase front as dependent on interlamellar spacing at a constant growth rate of $\Delta T = K_1\lambda V + \frac{K_2}{\lambda}$ *[21]*

Rys. 15. Przechłodzenie dwufazowego frontu krzepnięcia w zależności od odległości między płytkami przy stałej szybkości wzrostu fazy $\Delta T = K_1\lambda V + \frac{K_2}{\lambda}$ *[21]*

The critical lamellar spacing λ_e is determined by the thermodynamic driving force $\Delta G = V\,\Delta Gp + A\gamma$, necessary for progress of the process. In the analysed case, the released volume energy $V\Delta Gp$ resulting from replacing of Al_6FeMn phase by α-AlMnFeSi phase is progressively balanced by an increase in surface energy Aγ of the α-AlMnFeSi/Al interfaces. When the critical λ_e value is achieved, the peritectic two-phase zone growth is arrested, though volume increase of the α-AlFeMnSi phase is still thermodynamically favoured. The maximum value of lamellar spacing λ_{max} is limited by an increase in the diffusion distance of both Fe and Mn in the solid state.

The filigrees of α-AlMnFeSi phase observed in α-Al matrix, behind the L/α-AlMnFeSi profile have seemed to be a prolongation of some lamellae from the peritectic zone (Figs. 5e–f, 6b, 11, 14). No thermal effects that could be ascribed to this process have been recorded during calorimetric analysis, but a stepwise increase in the lamellar spacing reflects changes in the process course.

The filigrees formation should take place after the growth of the transformed zone inside an Al_6FeMn particle has been completed. Otherwise, the Si atoms necessary for the α-AlMnFeSi phase growth at an internal Al_6FeMn/α-AlMnFeSi front would have been consumed at the external Al_6FeMn/L interface. The lamellae branching changing into the Chinese script is characteristic of the precipitation of this phase in liquid alloy. Therefore, the filigrees growth occurs in the liquid alloy with kinetic domination of the α-AlMnFeSi phase over the α-Al solid solution solidification.

If the minimum undercooling criterion [22]:

$$\lambda = \frac{(2ma_p)}{\Delta T}$$

(where: m – liquidus slope, a_p – geometry coefficient)

is applied, then the observed change in the external λ spacing can be ascribed to the decrease of local undercooling due to recalescence (the delivery of latent heat of transformation) at the front of growth.

However, the filigrees growth demands not only silicon but also transition metals transport at the α-AlFeMnSi/α-Al interface from the subsequent zones of liquid alloy.

Though the diffusivity of both Fe and Mn in liquid Al is only slightly faster than that of Si, their diffusion distance is much longer (Fig. 16). The volume of the liquid phase containing the number of transition atoms necessary to build one unit volume of the α-AlMnFeSi phase is about 6 times larger than that of the primary Al_6FeMn phase. The λ_p/λ_f ratio (Table 3) observed in the examined alloys has been estimated as comprised in a range of 4(Mn + Fe = 4.5%) ÷ 8(Mn + Fe = 3.5%), which can be compared with the concentration relation: $\%(Mn + Fe)_{Al6FeMn} / \%(Mn + Fe)_{alloy}$. Thus, the growth of external filigrees of the α-AlFeMnSi phase occurs in the liquid at the expense of components which have remained in it after the transformation in a primary particle has ended. The local concentration of transition metals and of silicon around the peritectically transformed precipitates will

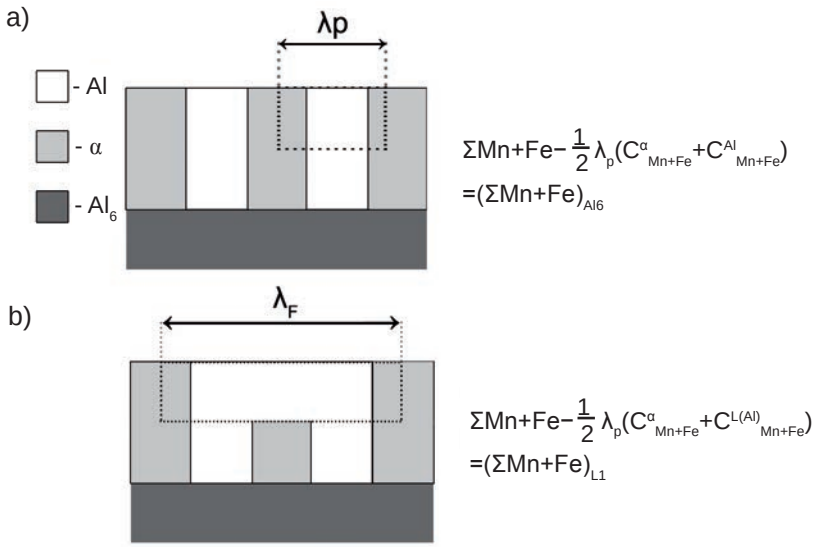

Fig. 16. The formation of filigrees zone and elements content in the microregion of AlMnFeSi lamellae + α-Al in both areas: a) peritectic layer V_v^{ap}, and b) filigrees zone V_v^{aF}, when assumed $V_v^{ap} = V_v^{aF}$ (ΣMn + Fe - transition metals content in marked microregion), $(\Sigma Mn + Fe)_{Al6}$ - transition metals content in Al_6FeMn phase, $(\Sigma Mn+Fe)_{L1}$ - transition metals content in liquid solution, λ_p - interlamellar distance in internal peritectic layer, λ_F - interlamellar distance in external layer(filigrees), C^{α}_{Mn+Fe} - transition metals content in α-AlMnFeSi phase, C^{Al}_{Mn+Fe} - transition metals content in α-Al solid solution in two-phase layer, $C^{L(Al)}_{Mn+Fe}$ - transition metals content α-Al solid solution round the precipitate

Rys. 16. Powstawanie obszaru struktury chińskiego pisma oraz zawartość pierwiastków w mikroobszarze struktury płytkowej AlMnFeSi + α-Al w obu strefach: a) warstwa perytektyczna V_v^{ap} i b) obszar struktury chińskiego pisma V_v^{aF}; przy założeniu $V_v^{ap} = V_v^{aF}$, ΣMn+Fe - zawartość metali przejściowych w oznaczonym mikroobszarze, $(\Sigma Mn + Fe)Al_6$ - zawartość metali przejściowych w fazie Al_6FeMn, $(\Sigma Mn + Fe)_{L1}$ - zawartość metali przejściowych w ciekłym roztworze, λ_p - odległość międzypłytkowa w wewnętrznej warstwie perytektycznej, λ_F - odległość międzypłytkowa w warstwie zewnętrznej (obszar struktury chińskiego pisma), C^{α}_{Mn+Fe} - zawartość metali przejściowych w fazie α-AlMnFeSi, C^{Al}_{Mn+Fe} - zawartość metali przejściowych w stałym roztworze α-Al w warstwie dwufazowej, $C^{L(Al)}_{Mn+Fe}$ - zawartość metali przejściowych w stałym roztworze α-Al dookoła wydzieleń)

3.2.4. The diffusion transport of components within peritectic layer

The formation of a concentration gradient of components across the peritectic layer thickness is usually very limited due to a narrow range of tolerance for the fluctuations in composition of the intermetallic phase.

As the process occurs *in situ* and the content of transition metals in both primary and peritectic phases is well-balanced, the transfer of transition metals is considered to be limited only to an interlamellar spacing.

Instead, a strong deficiency of Si occurs at the α-AlFeMnSi/Al_6FeMn interface. Depending on the accepted formula of the α-AlFeMnSi phase, the range of ΔSi is about 6–8 wt.% (Fig. 13).

When the lattice diffusion mechanism is assumed, the Si diffusion driving force is determined by the concentration gradient between both external and internal boundaries of the peritectic layer: $\Delta C_{Si} = C_{\alpha c/L}^{si} - C_{Al6/\alpha c}^{Si}$.

According to the peritectic growth law based on Wagner formula, the growth rate Δx /t dependence on the Si concentration gradient [12,13] will be expressed by the following formula:

$(\Delta x)^2 = 2t\gamma D\Delta C_{Si}$.

In the two-phase particles formed during homogenisation examined by Alexander, no Si gradient was revealed. The size of particles was small compared to the estimated distance of Si transfer, achieved when the process occurred (e.g. at 600°C/1 h – 150 μm, [10, 11]. Therefore, the A-type lattice diffusion of silicon should be sufficient transport means for this element to feed and drive the transformation on the whole cross-section of the primary particle.

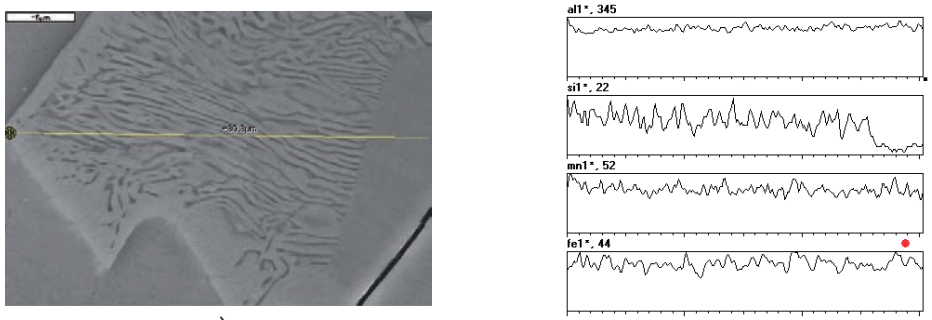

a) b)

Fig. 17. Distribution of components between the primary and peritectic phases in AlFeSiMn alloy, a) SEM, etched with 1% HF, 7000x, b) concentration profile of components along the peritectic layer

Rys. 17. Rozkład składników pomiędzy fazami pierwotnymi i fazami perytektycznymi w stopie AlFeSiMn, a) skaningowa mikroskopia elektronowa, trawienie 1% HF, pow. 7000x. b) profil stężenia składników wzdłuż warstwy perytektycznej

In the examined specimens, a small Si concentration gradient was observed within the peritectic layer formed during slow cooling (Fig. 17). The average difference in Si concentration between the external and internal layer boundaries was in the range of 0.2–0.3 wt.% (the layer thickness of at least 20 μm). This result estimated by EDS microanalysis was statistically proved to be at a 95% confidence level (Fig. 18).

Since the transformed layer thickness observed in the examined specimens has achieved its maximum value comparable with the one obtained after a homogenisation process, a similar Si diffusion mechanism could be assumed.

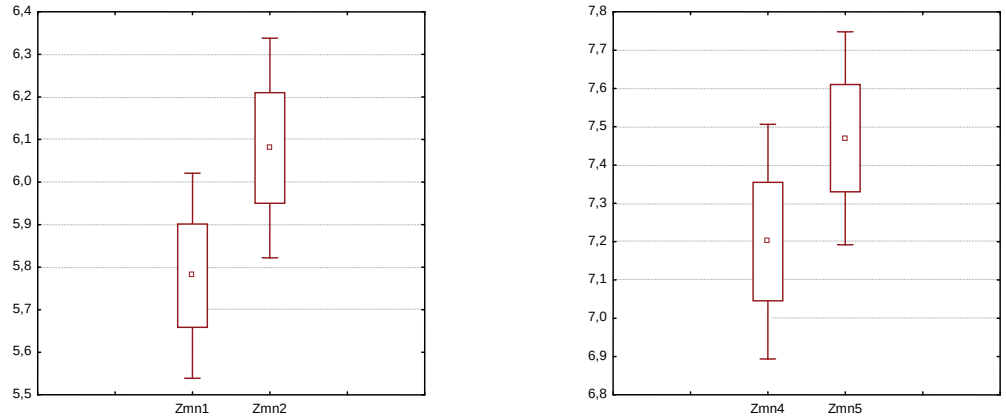

a) b)

Rys. 18. Silicon gradient in the peritectic layer (at. %); a) Si0.5, Fe/Mn 0.75, b) Si2.5 Fe/Mn0.75 (left bar – C^{Si} at the internal growth front, right bar – C^{Si} at the external microregion of a peritectic layer)

Rys. 18. Gradient zawartości krzemu w warstwie perytektycznej (% at.); a) Si0,5, Fe/Mn 0,75, b) Si2,5 Fe/Mn0,75 (słupek lewy – C^{Si} na wewnętrznym froncie wzrostu, słupek prawy – C^{Si} w zewnętrznych mikroobszarach warstwy perytektycznej)

3.3. The redistribution of transition metals between intermetallic phases

The stable chemical composition of intermetallic phases is one of their specific features governed by Hume-Rothery rules. Nevertheless, the chemical composition of both the Al_6FeMn and α-AlFeMnSi phases formed in aluminium alloys as a substitution solid solution is, in general, strongly influenced by alloy composition.

In particular, it is the Fe/Mn ratio in alloy that governs the thermodynamic stability. When Fe dissolves in the base phase lattice, an array of the solid solution forms.

In the primary Al_6Mn phase, an increase in the dissolved Fe content leads to changes in the crystal space group (from Ccmm (Al_6Mn) to $Cmc2_1$ (Al_6Fe) [25], and then the phase loses its thermodynamic stability:

Stable Al_6Mn + Fe → Al_6FeMn + Fe → metastable Al_6Fe

The equilibrium Fe/Mn ratio is considered equal to 1, but some authors have reported larger Fe ↔ Mn replacements even in the range of about 56% [2].

The possible extent of the Fe ↔ Mn replacement in a regular α-AlFeMnSi phase is very large (Fe → Mn of about 95%), but if the Fe content exceeds certain concentration limit, the new hexagonal α-AlFe(Mn)Si phase becomes thermodynamically favoured [5]. This concentration limit in the phase is not exactly determined, but estimated on the ground of several reference studies as comprised in a range of 0.3–0.5 wt.%.

Figure 19 shows the distribution of transition metals between the precipitates of intermetallic phases formed at the subsequent stages of peritectic crystallisation, examined in specimens cooled at a rate of 5 K/min.

The maximum value of Fe/Mn ratio (about 1.3) observed in the Al_6FeMn primary precipitates in both hypo- and near-peritectic phases has been slightly higher than the level considered equilibrium in this phase but lower than that reported in studies carried outpreviously on this alloy. It means that the range of Fe ↔ Mn replacement in the examined specimens has been wider than that reported previously. At the temperature of the Al_6FeMn phase precipitation, two factors, i.e. either higher Fe diffusivity or its lower (compared with Mn) solubility in liquid alloy, can promote the Fe accumulation in primary particles.

A small increase in the Mn content has been noticed in the peritectic layer, while the *in situ* mechanism of the new phase building is a rather exact copy of the Fe/Mn ratio in the primary phase. However, a tendency similar to Mn diffusion into the α-AlFeMnSi phase precipitates has been stated by several authors in the technical alloys after heat treatment [15, 16]. Though the direct reason of this phenomenon has not be recognised yet, the expected decrease in Fe/Mn ratio at the Al_6FeMn/L interface around the primary precipitates can be considered the driving force for local Mn gradient balance.

A very high Fe concentration in the α-AlFeMnSi phase filigrees, formed at a terminal stage of the peritectic precipitation has resulted from a very low value of the partition coefficient at an α-Al/L interface, compared to that of Mn.

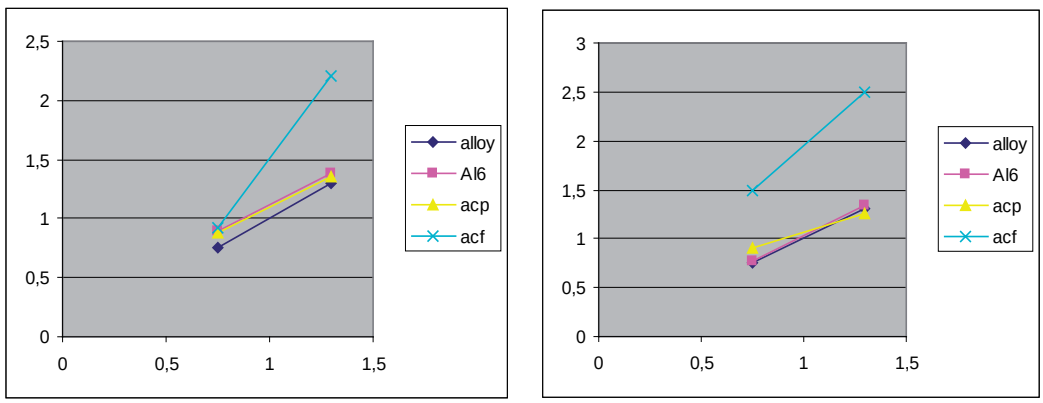

a) b)

Fig. 19. The redistribution of transition metals between intermetallic phases, a) Fe/Mn ratio in alloys with 0.5 wt.% Si, b) Fe/Mn ratio in alloys with 2.5 wt.% Si

Rys. 19. Ponowny rozkład metali przejściowych pomiędzy fazami międzymetalicznymi, a) stosunek Fe/Mn w stopach z zawartością 0,5% wag. Si, b) stosunek Fe/Mn w stopach z zawartością 2,5% wag. Si

Thus, the Fe/Mn ratio in each of the intermetallic phases precipitate has been influenced by the following factors:

- the Fe/Mn ratio in the alloy,
- the limit of the equilibrium Fe/Mn ratio in particular phases,
- the evolution in liquid alloy composition during progress in the process.

4. Summary and conclusions

1. The course of the peritectic L + $Al_6Mn(Fe)$ → α-Al + α-AlMnFeSi transformation, identified in the examined alloys, was described on the ground of the results obtained by local methods of investigation. The two-phase α-Al + α-AlMnFeSi lamellar structure in a peritectic product layer was revealed by observations under the microscope (LM and SEM) and identified by means of both EBSD and EDS microanalyses.
2. The peritectic formation of the α-AlFeMnSi phase occurs in two microareas:

   a) inside the primary Al_6FeMn phase precipitates

   A lamellar two-phase layer grows at the expense of Fe, Mn and Al atoms from the Al_6FeMn matrix and Si atoms transported from the liquid alloy.

The Fe, Mn and Al diffusion distance is comparable with the lamellar spacing and parallel to the growth front at the Al_6FeMn/α-AlFeMnSi interface.
Silicon is supplied from liquid alloy and its flux is perpendicular to the growth front at an Al_6FeMn/α-AlFeMnSi interface. Though the α-AlFeMnSi/α-Al interfaces seem to be the favourable diffusion paths, the Si concentration gradient in the transformed layer can be the source of a driving force of the lattice diffusion. The effectiveness of a given diffusion mechanism has not been verified because of the lack of data on material constants.

b) outside the primary Al_6FeMn phase precipitates

The α-AlFeMnSi phase filigrees have been formed in liquid alloy owing to the consumption of its components. The lamellar distance has been controlled by the Fe and Mn diffusion efficiency in the liquid. This stage of the process can develop until a direct α-AlFeMnSi/L contact is maintained.

3. The nucleation of the α-AlFeMnSi phase has been recognised as a controlling factor at the stage of peritectic reaction. When the process passes into a transformation stage, the growth kinetics becomes the predominant control factor.
4. The distribution of transition metals between both intermetallic phases reflects the Fe/Mn ratio in the examined alloy. However, the Fe tendency to accumulate in both Al_6FeMn phase precipitates and external filigrees of the α-AlFeMnSi phase has been noticed, accompanied by a relative Mn content increase in the two-phase layer. It can be promoted by differences in either diffusivity or partition coefficient of these elements in the intermetallic phases involved in the process.

Acknowledgments

This work has been executed owing to a financial support of the Polish Ministry of Science and Higher Education under grants Nos. 4 T08B 03222 and 3787/B/T02/2008/35. Author would like to thank dr A. Gazda from Foundry Research Institute for DSC experiments and dr S. Boczkal from OML IMN Skawina for EBSD analysis.

References

1. Yong Du et al.: A Thermodynamic description of the Al-Mn-Si system over the entire composition and temperature ranges, Met. and Mat. Transactions A, 2004, Vol. 35, No. 5, pp. 1613–1626.
2. Phragmen G.: On the phases occurring in alloys of aluminium with copper, magnesium, manganese, iron, and silicon, Journal of the Institute of Metals, 1950, Vol. 77, pp. 489–552.
3. Barlock J.G., Mondolfo L.: Structure of some aluminium-iron-magnesium-manganese-silicon alloys, Z. Metallkunde, 1975, Vol. 66, pp. 605–611.
4. Balitchev E., Jantzen T., Hurtado I., Neuschuts D.: Thermodynamic assesment of the quaternary system Al-Fe-Mn-Si in the Al-rich corner, Computer Coupling of Phase Diagrams and Thermochemistry, 2003, Vol. 27, No. 3, pp. 275–278.
5. Yong Du at al.: Thermodynamic description of the Al-Fe-Mg-Mn-Si system and investigation of microstructure and microsegregation during directional solidification of an Al-Fe-Mg-Mn-Si alloy, Z. Metallkunde, 2005, Vol. 96, pp. 1351–1362.
6. Backerud L., Krol E.,Tamminen J.: Solidification Characteristics of Aluminium Alloys. Volume 1: Wrought Alloys, Skanaluminium, Oslo, 1986.
7. Alexander D.T.L., Greer A.L: Solid state intermetallic phase transformations in 3XXX aluminium alloys, Acta Mat., 2002, Vol. 50, No. 10, pp. 2571–2583.
8. Alexander D.T.L et al.: Study of intermetallic phase transformations in 3XXX alloys using diffusion couples, Materials Science Forum, 2002, Vols. 396–402, 681–686.

9. Alexander D.T.L., Greer A.L: Nucleation of the Al_6(Fe,Mn)-to-α-Al(Fe,Mn)-Si transformation in 3XXX aluminium alloys. II. Transformation in cast aluminium alloys, Phil. Mag., 2004, Vol. 84, No. 28, pp. 3071–3083.
10. Alexander D.T.L., Greer A.L.: Nucleation of the Al_6(Fe,Mn)-to-α-Al(Fe,Mn)-Si transformation in 3XXX aluminium alloys. I. Roll-bonded diffusion couples, Phil. Mag., 2004, Vol. 84, No. 28, pp. 3051–3071.
11. Li Y.J., Arnberg L.: A eutectoid transformation for the primary intermetallic particle from Al_m(Fe,Mn) to Al_3(Fe,Mn) in AA5182, Acta Mat., 2004, Vol. 52, No. 10, pp. 2945–2952.
12. St. John D.H., Hogan L.M.: The peritectic transformation, Acta Met., 1977, Vol. 25, No. 10, pp. 77–81.
13. Sartell J.A., Mack D.J.: The mechanism of peritectic reactions, Journal of Institute of Metals, 93, (1964–65), pp. 19–24.
14. Fredriksson H., Nylén T.: Mechanism of peritectic reactions and transformations, Journal of Metal Science, 1982, Vol. 16, No. 6, pp. 283–294
15. Warmuzek M., Mrówka G., Sieniawski J.: Influence of heat treatment on the precipitation of the intermetallic phases in commercial AlMn1FeSi alloy, J. Mat. Proc. Tech., 2004, Vol. 157–158C, pp. 624–626.
16. Warmuzek M., Gazda A.: An analysis of cooling rate influence on the sequence of intermetallic phases precipitation in some commercial aluminium alloys, J. of Analytical Atomic Spectrometry, 1999, Vol. 14, pp. 535–537.
17. Jasna B., Bonderek Z., Warmuzek M.: Intermetallic phases formed in Al-Fe-X-Si alloys (where X-Mn, Cu). Proc. of the 14th Conference on Applied Crystallography, Cieszyn, 22–26 August, 1994.
18. Watanabe H., Ohori K., Takeushi Y.: Phasenumwandlung in AlMn1Mg1–Legierungen bei gesteigerten Temperaturen, Aluminium, 1984, Vol. 60, pp. 373–376.
19. Jeniski R.A., Thanaboonsombut B., Sanders T.H.: The effect of iron and manganese on the recrystallization behavior of hot-rolled and solution-heat-treated aluminium alloy 6013, Met. and Mat. Trans. A, 1996, Vol. 27A, No. 1, pp. 19–27.
20. Kaczyński J., Prowans S.: Podstawy teoretyczne metaloznawstwa, Wyd. Śląsk, Katowice, 1972.
21. Aguiar M.R., Caram R.: Lamellar spacing selection in a directionally solidified Sn-Se eutectic alloy, J. of Cryst. Growth, 1997, Vol. 174, No. 1–4, pp. 70–75.
22. Fraś E.: Krystalizacja metali i stopów, Wyd. Naukowe PWN, Warszawa, 1992.
23. Donnadieu D. et al.: Alpha-phase particles in 6XXX aluminium alloys, Proc. 4th International Conference on Aluminum Alloys, USA, Atlanta, 11–16 September 1994, pp. 668–675.
24. Jackson K.A., Hunt J.D.: Lamellar and rod eutectic growth, Trans. Met. Soc. AIME, 1966, No. 236, pp. 1129–1142.
25. Nicol A.D.I.: The structure of $MnAl_6$, Acta Cryst., 1953, Vol. 6, No 3, 285–293.